ACS APPLIED ELECTRONIC MATERIALS

pubs.acs.org/acsaelm Letter

Coalescence of GaP on V-Groove Si Substrates

Theresa E. Saenz, John S. Mangum, Olivia D. Schneble, Anica N. Neumann, Ryan M. France, William E. McMahon, Jeramy D. Zimmerman, and Emily L. Warren*

Cite This: ACS Appl. Electron. Mater. 2023, 5, 721−728 Read Online

ACCESS | Metrics & More | Article Recommendations | Supporting Information

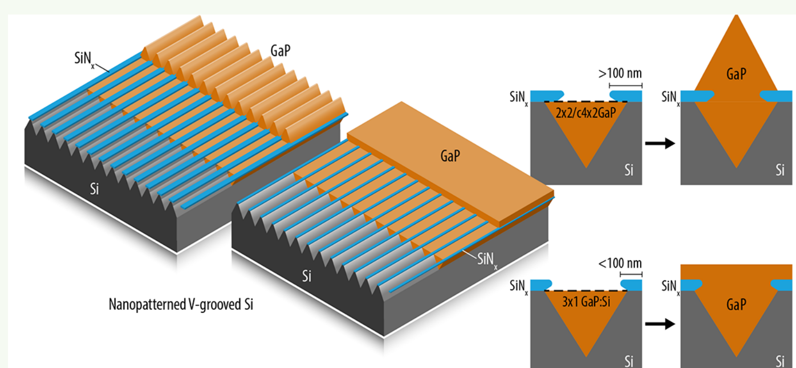

ABSTRACT: Here, we study the morphology and dislocation dynamics of metalorganic vapor phase epitaxy (MOVPE)-grown GaP on a V-groove Si substrate. We show that Si from the substrate stabilizes the (0 0 1) GaP facet, which is critical for achieving coalescence. The SiN_x caps covering the (0 0 1) tops of the V-grooves must be sufficiently small for the 3 × 1 GaP surface reconstruction caused by Si to continue to influence the GaP coalescence while the V-grooved sidewalls are covered. If the SiN_x caps are too large, (1 1 1) diamond faceting develops in the GaP, and coalescence does not occur. On samples where coalescence is successful, we measure a root-mean-square roughness of 0.2 nm and a threading dislocation density of 5×10^7 cm^{-2}. Dislocation glide was found to begin during coalescence through transmission electron microscopy. With further TDD reduction, these GaP on V-groove templates will be suitable for III-V optoelectronic device growth.

KEYWORDS: *MOVPE growth, III-V on Si, heteroepitaxy, thin films, nanopatterning*

Downloaded via NATL RENEWABLE ENERGY LABORATORY on March 3, 2023 at 19:23:50 (UTC).
See https://pubs.acs.org/sharingguidelines for options on how to legitimately share published articles.

The direct growth of high-quality III-V semiconductors on Si substrates for optoelectronic devices has been a key research goal for decades. Recently, advances in the control of crystalline defects in the epitaxial III-V layers[1−11] has enabled rapid performance increases for III-V-on-Si solar cells[12−14] and lasers.[15−18] V-groove Si, a type of selective area growth (a strategy used in many epitaxial systems[19−24]) where a substrate uses selective etching of nanopatterns to produce {1 1 1}-faceted trenches on a (0 0 1)-oriented Si wafer, is one of the technologies that has enabled this progress.[25,26] The {1 1 1}-faceted surface of these templates stops the formation of antiphase domains (APDs), which historically have been a persistent problem for III-V-on-Si growth. V-grooves have been used for the direct growth of GaAs,[27−32] InP,[33−36] GaSb,[37] and GaP[38−41] on Si for laser and solar cell applications via metalorganic vapor phase epitaxy (MOVPE). We previously studied the nucleation of GaP on V-groove Si and identified suitable high-temperature growth conditions for GaP nucleation.[40] In this work, we explore the coalescence of MOVPE-grown GaP on V-groove Si to establish a suitable III-V-on-Si template for optoelectronic device growth.

For applications requiring continuous, large-area III-V thin films, V-groove Si adds a degree of complexity that is not present for growth on planar substrates or selective area growth not requiring thin films. Namely, material nucleated in neighboring grooves must coalesce to form a thin film. As opposed to conventional thin-film growth on planar substrates, conformal growth on the V-groove substrate is not always desired. For films grown by MOVPE, lateral growth is typically encouraged with a high V/III ratio to promote coalescence when growing over nanopatterns.[21,27,42] Additionally, the dislocation dynamics differs between a V-groove system and planar substrates. The coalescence of relaxed, lattice-mismatched material can drive the formation of grown-in, sessile threading dislocations.[43] Additionally, the shape of the

Received: December 12, 2022
Accepted: February 14, 2023
Published: February 16, 2023

ACS Publications

© 2023 The Authors. Published by American Chemical Society

https://doi.org/10.1021/acsaelm.2c01688
ACS Appl. Electron. Mater. 2023, 5, 721−728

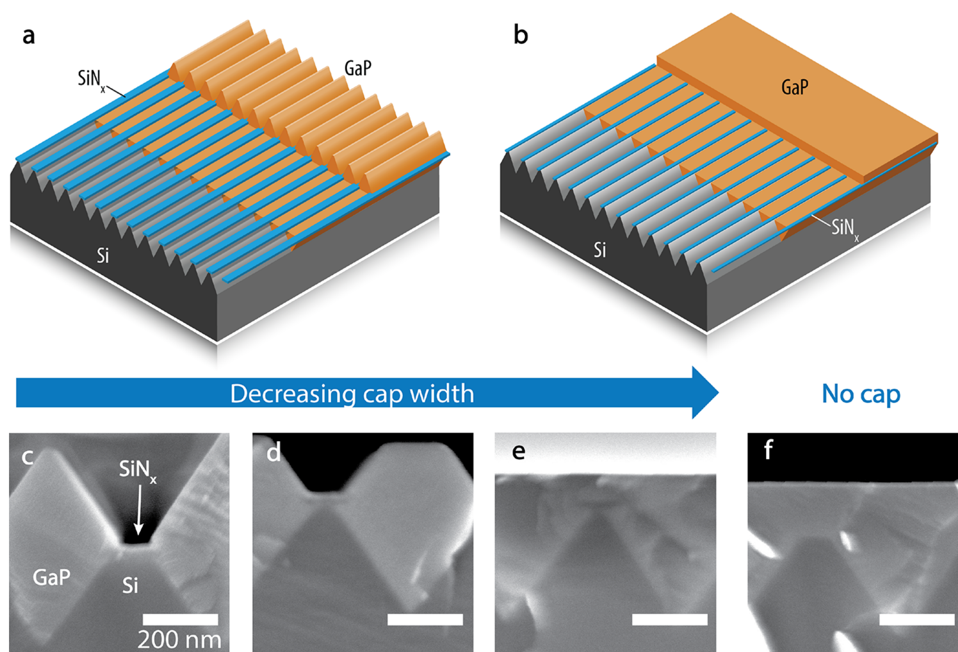

Figure 1. (a,b) Schematics of GaP on V-groove Si with a (1 1 1) diamond morphology (a) and a coalesced (0 0 1) morphology (b). (c−f) SEM cross-sectional images of GaP grown on Si, with varying SiN_x cap widths on V-grooves with a 500 nm spatial period. Diamond morphologies are produced for larger cap widths (a,b), whereas flat morphologies are produced when the SiN_x cap is under 100 nm wide (c) or not present (d). All samples were grown together in the same run (WB989) at T_g = 800 °C and V/III = 5000.

V-grooves changes the strain profile in the III-V material and thus the driving force for dislocation glide.[44]

This work seeks to understand the evolution of morphology and defects during the coalescence of MOVPE-grown GaP on V-groove Si. Due to the relatively small lattice mismatch between GaP and Si (0.4% mismatch), this heteroepitaxial system allows us to focus on the impact of the V-groove morphology without the large lattice mismatch that is present in other III-V materials that have grown on V-groove Si, e.g., GaAs (4% mismatch)[27−31] and InP (8% mismatch).[33−36] We discuss the effects of the substrate geometry on the resulting coalesced material and propose a mechanism for the observed behavior. Additionally, we study the dislocation dynamics and strain relaxation of the GaP before and after coalescence. Using SiN_x hard mask caps to fabricate the V-groove leads to smooth coalescence when they are ≤100 nm wide and demonstrates that Si from the V-groove sidewalls stabilizes the (0 0 1) GaP surface and produces smooth coalescence. We demonstrate coalesced GaP on V-groove Si thin films with a root-mean-square roughness (R_q) of 0.2 nm, measured by atomic force microscopy (AFM), and a threading dislocation density (TDD) of 5×10^7 cm^{-2}, measured by electron channeling contrast imaging (ECCI).

V-groove substrates introduce a number of variables that can influence III-V nucleation that are not present on conventional chemomechanically polished (CMP) Si substrates. These include the exact geometry of the nanostructures,[45] the spatial period of the grooves, the direction of any substrate offcut relative to the grooves, and any deviation in the alignment of the V-grooves relative to the [1 1 0] direction. In this work, we investigated the impact of the SiN_x cap dimensions on the coalescence process. We produced V-groove samples with SiN_x caps ranging from 100−140 nm in width as well as a sample without a cap, leaving an exposed (0 0 1) Si surface at the top of the grooves. Then, GaP was nucleated and grown on the samples by MOVPE for 50 min with the optimized conditions described in the experimental section.

The scanning electron microscopy (SEM) cross-sectional images in Figure 1 show a transition from (1 1 1)-faceted GaP growth[41] to (0 0 1)-faceted GaP coalescence as the SiN_x caps decrease in width. We observe that for caps less than 100 nm wide or for samples with no caps, the GaP coalesces into a thin film. For samples with a wider SiN_x cap, the GaP develops a diamond-like morphology with {1 1 1} faceting after it fills the grooves and does not coalesce. We always observed (0 0 1)-faceted growth in the V-groove trenches, regardless of cap width. We investigated a number of additional factors as possible variables controlling morphological evolution; we observed that the reactor history, the magnitude of sample offcut, direction relative to the V-grooves, and the details of the wet chemical and AsH_3 pretreatments had no effect on the morphological evolution of GaP as it grew over the V-grooves. The role of the cap thickness was not investigated here but is expected to follow a trend with some maximum thickness beyond which the GaP does not coalesce.

One factor that changes between growth within the v-grooves and growth after filling is the presence of the exposed Si substrate. The change in GaP faceting upon the complete filling of the V-grooves points to a change in the surface energy of the (0 0 1) GaP surface at that point in the growth. At the high temperature at which the GaP is grown, it is likely that the Si from the exposed sidewalls is transported to the GaP surface via vapor phase transport and/or surface diffusion. Once the Si sidewalls are covered with GaP, there is no longer a source of surface Si present. As Si has been observed to influence the surface reconstruction of GaP,[46] we hypothesize that the mobile Si supplied from the V-groove sidewalls stabilizes the (0 0 1) facet.

To more directly study the effect of Si on the GaP surface, we carried out a series of three experiments using Si_2H_6 flow

https://doi.org/10.1021/acsaelm.2c01688
ACS Appl. Electron. Mater. 2023, 5, 721−728

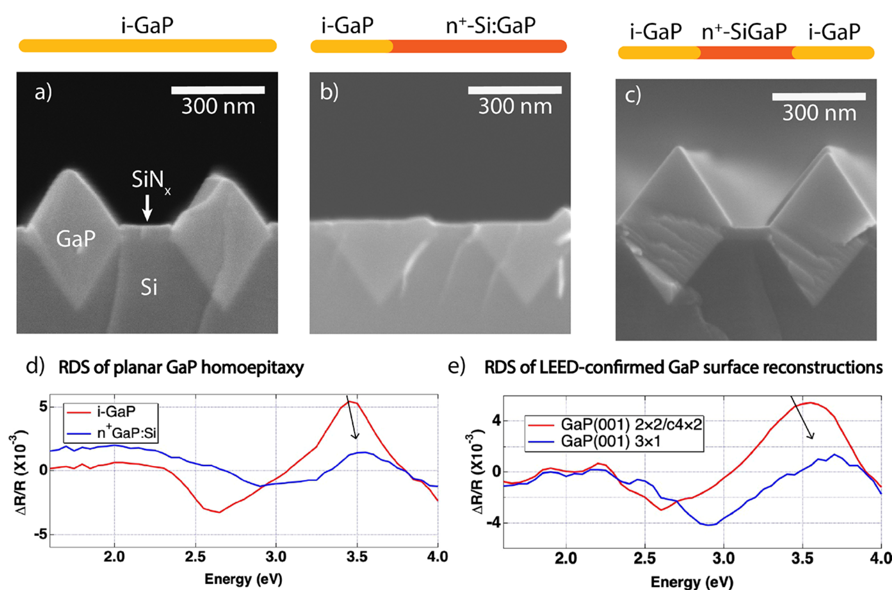

Figure 2. (a−c) SEM cross-sectional images of GaP on V-groove Si comparing the impact of adding external Si dopants. All samples were grown under the same V/III ratio and temperature for the same length of growth time (V/III = 5000, T_g = 800 °C, time = 42 min). The bars above the images visually represent the flow of Si over the course of growth. Sample (a) was grown without Si_2H_6 (WC206); sample (b) had Si_2H_6 at the end of growth (WC150); and sample (c) had the Si source flowing for part of the growth (WC174). These three samples suggest that Si on the GaP growth surface suppresses the formation of {1 1 1} GaP facets. (d) shows RDS measured on homoepitaxial GaP wafers using the same growth conditions as for V-groove growth (WC323). (e) shows the RDS of a standard 2 × 2/c4 × 2 and a Si-contaminated 3 × 1 (0 0 1) GaP surface reconstruction from a previous study,[46] where the surface reconstructions were confirmed with LEED (PC178).

during GaP growth to mimic the effect of Si transport onto the GaP surface from the V-groove sidewalls. The SiN_x caps for these samples were 200 nm wide, ensuring that growth would be expected to have the diamond morphology at our standard growth conditions. All growth began with unintentionally doped GaP nucleation and growth in order to avoid influencing the nucleation process. After 12 min, the V-grooves were about $\frac{1}{2}$-filled with GaP, with exposed Si sidewalls remaining above the (0 0 1) GaP growth front (Figure S1a). After 30 min of growth, the V-grooves were completely filled (but not overgrown) with GaP still with an (0 0 1) surface (Figure S2b). For sample a, unintentionally doped GaP was grown for the entire 42 min (Figure 2a). For sample b (Figure 2b), unintentionally doped GaP was grown for 12 min, followed by GaP:Si under Si_2H_6 for 30 min to provide excess Si even after the sidewalls were covered. For sample c, unintentionally doped GaP was grown for 12 min, followed by GaP:Si under Si_2H_6 for 20 min, followed by unintentionally doped GaP for the final 10 min to show the morphology that forms without excess Si present. All three of these samples were grown for the same amount of time, with the same Ga flow throughout, at T_g = 800 °C and V/III = 5000. The 42 min of GaP growth used here provides sufficient time for the GaP to coalesce for samples with narrow caps.

SEM cross-sectional imaging (Figure 2) shows that the control sample (a) has the expected diamond morphology. The sample exposed to Si doping throughout the later portion of growth (b) did not coalesce into a thin film nor did it develop diamond faceting. This sample retained its (0 0 1) GaP faceting, with growth filling the grooves and then stopping. Finally, for the sample where Si doping was turned on and off again (c), the growth developed a diamond morphology. These results suggest, as hypothesized, that (1) Si stabilizes the (0 0 1) GaP facet at the growth conditions used in this work and (2) this effect can be reversed by removing the Si source. Intermediate growth steps after 12 and 32 min without any Si_2H_6 flowing are shown in the Supporting Information (S1).

Previous work has shown that the presence of some Group IV elements, such as Si and Ge, can produce a 3 × 1 surface reconstruction on III-Vs that results in a chemically inert (0 0 1) surface.[46] Work on GaAs nanowires has also shown that dopant level Si can have a stabilizing effect on certain facets.[47] In the current work, we observe a correlation between (0 0 1) GaP faceting and the supply of Si atoms to the GaP surface, and we hypothesize that these (0 0 1) GaP facets are similarly stabilized by Si atoms at the GaP surface. In this case, the Si could be supplied from the exposed Si surfaces until the grooves are filled with GaP. Our prior work was done on a growth reactor connected to an ultra-high-vacuum (UHV) chamber, enabling low-energy electron diffraction (LEED), scanning tunneing microscopy (STM), and Auger electron spectroscopy studies of the resulting 3 × 1 surface reconstruction.[46] The current work was done in a stand-alone MOCVD chamber without these capabilities; however, both MOCVD chambers have in situ reflectance difference spectroscopy (RDS), providing a connection between current and prior work. A comparison was done using GaP (001) surfaces grown homoepitaxially on GaP substrates to avoid complications due to optical diffraction from the V-groove Si. GaP layers were grown both with and without Si doping, using the same Si flow as the experiments shown in Figure 2 at the optimized growth conditions described in the experimental section. Between layers, the wafer was cooled to 350 °C to measure RDS.

Figure 2d shows the RDS measurement from our current work. As a comparison, Figure 2e shows the RDS of a LEED-confirmed Si-contaminated 3 × 1 (0 0 1) GaP surface reconstruction and the RDS of a standard 2 × 2/c4 × 2 (0 0 1)

https://doi.org/10.1021/acsaelm.2c01688
ACS Appl. Electron. Mater. 2023, 5, 721−728

GaP surface reconstruction that was acquired for a previous study[46] but not previously published. The RDS shows a decrease in intensity and a shift to higher energies of the peaks for the Si-doped GaP compared to the intrinsic GaP. This same shift is observed for 3×1 GaP compared to $2 \times 2/c4 \times 2$ GaP, suggesting that the high Si_2H_6 flow induces a 3×1 reconstruction on the GaP.

We suggest that this surface reconstruction, induced by a large amount of Si from the V-groove sidewalls (or intentionally by high levels of dopant flow), is the mechanism by which the (0 0 1) GaP facet is stabilized for growth in the grooves. A possible kinetic picture of this process is as follows: on the {1 1 1} Si sidewalls, Ga species can adsorb, but no GaP growth occurs there, as shown in previous work.[40] Concurrently, on the 3×1 GaP surface, no Ga adsorption can occur, but GaP growth can occur as Ga migrates from the Si sidewalls. When the groove is filled, the source of Si is removed, resulting in a different surface reconstruction and thus allowing {1 1 1} GaP facets to develop. If instead Si continues to be supplied via dopant flow, then growth stops entirely, as there is no surface to which Ga readily adsorbs. For a sample where thin-film coalescence occurs, the coalescence likely takes place during a transient period associated with an intermediate level of residual Si on the growth surface that maintains stable (0 0 1) facets but does not bring the Ga sticking coefficient on GaP to zero. This would explain why the SiN_x must be sufficiently narrow for coalescence: there is likely only a small window where this transient condition could facilitate coalescence. The high-temperature GaP growth conditions, which produce exposed Si sidewalls, are key to this effect—if GaP growth began conformally, as is typical of low-temperature nucleation, we would not expect to see the stabilization of the {1 1 1} GaP facets.

Given this ability to control GaP coalescence on V-groove Si, we studied the material quality of these thin films further to evaluate their suitability for use as virtual III-V substrates for III-V optoelectronic device fabrication. Using AFM, we studied the roughness of a GaP thin film on a V-groove sample with SiN_x caps, as shown in Figure 3. A to-scale cross-sectional SEM image properly aligned with the AFM image of this sample is also shown as an inset. The root-mean-square roughness (R_q) over a 25 μm^2 area of the film was 0.2 nm. In comparison, the starting roughness of the CMP Si used to fabricate our V-groove Si was 0.1 nm. In addition, Hool et al.[4,10] achieved an R_q of 0.6 nm for 500 nm of GaP grown on offcut, CMP Si without any nanopatterning, and Li et al.[27] reported an R_q of 1.9 nm for a 300 nm coalesced GaAs on V-groove Si film. The steps visible on the image are a either 0.3 or 0.6 nm in height, consistent with monatomic or diatomic GaP steps. The V-groove caps are also visible through the GaP, which could result from an electrostatic interaction of the tip with the dielectric caps through the thin GaP layer. This smooth coalescence demonstrates control of the GaP morphology from nucleation to the formation of a thin film and provides a suitable template for further device growth from the perspective of morphology.

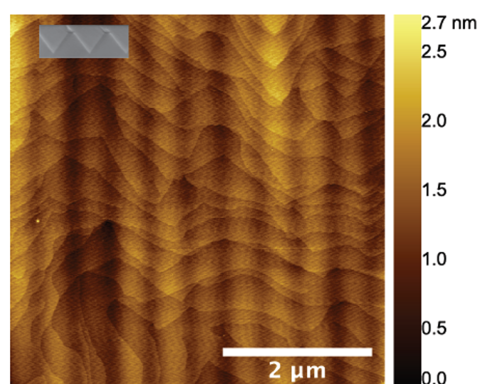

Figure 3. AFM of coalesced GaP on V-groove Si showing an R_q of 0.2 nm. The wavy steps observed have a height consistent with monatomic or diatomic GaP steps. The inset shows an SEM cross-sectional image of the same sample to scale, positioned to align with the AFM for orientation (WB430).

Defect density is also an important consideration for the use of these templates for optoelectronic device growth. For example, threading dislocations through active device layers are known to decrease III-V solar cell efficiency significantly if their density is higher than 10^6 cm^{-2}.[48] In addition to threading dislocations, ECCI can also identify planar defects such as stacking faults. ECCI was used in this study (Figure 4) to measure the TDD of coalesced GaP thin films with and without SiN_x caps as well as to identify any planar defects potentially associated with nucleation problems. For samples with SiN_x caps (Figure 4a, GaP thickness of 400 nm from the bottom of the groove, 70 nm from the top of the cap), the TDD is 5×10^7 cm^{-2}, measured from 115 dislocations counted over a 212 μm^2 area, and for samples without SiN_x caps (Figure 4b, GaP thickness of 400 nm from the bottom of the groove, 150 nm from the top of the groove), the TDD is 5×10^8 cm^{-2}, measured from 111 dislocations counted over a 23 μm^2 area. The ECCI shown for the sample with caps was previously reported,[41] but further analysis of this ECCI has revealed an additional feature: the lines running perpendicular to the grooves are likely misfit dislocations. In some cases, as indicated in Figure 4a, these misfits can be observed ending at threading dislocations. Some of the lines appear light, and others appear dark, as is expected for misfit dislocations of opposite Burgers vectors.[49] The continuity of these misfits across many neighboring grooves suggests that they result from dislocations gliding in after coalescence.

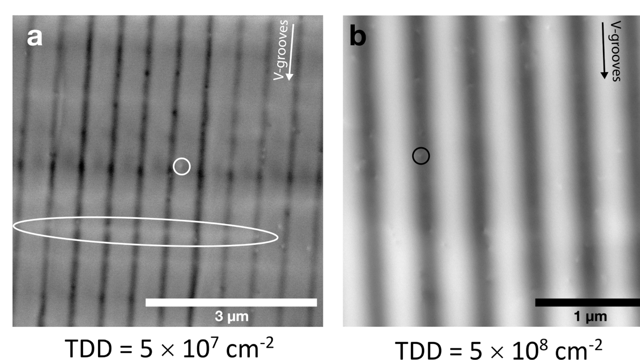

Figure 4. ECCI of coalesced GaP on V-groove templates with (a) and without (b) SiN_x caps. In (a), TDD ≈ 5×10^7 cm^{-2} (WB430), and in (b), TDD ≈ 5×10^8 cm^{-2} (WB989). An example of a threading dislocation is circled in each, and a misfit ending at a threading dislocation is circled in (a). No planar defects or associated pits are observed in the cap-free sample, unlike in previous work,[40] but the TDD remains elevated compared to the sample with caps. The direction of the V-grooves is marked with an arrow. (a) is reproduced from ref 41 with permission from IEEE. Copyright IEEE 2021.

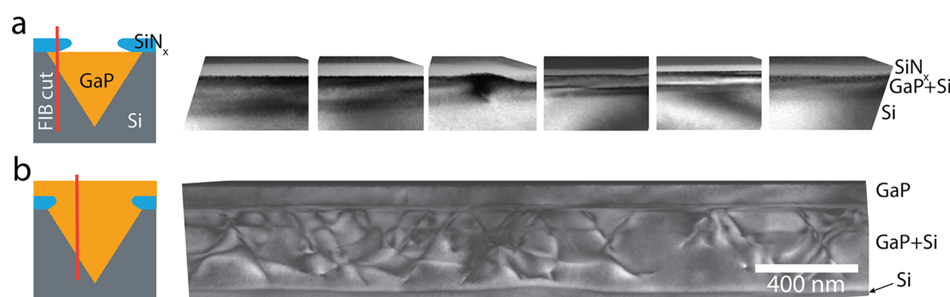

Figure 5. TEM of a focus ion beam (FIB) cross section prepared parallel to the V-grooves, showing a portion of the GaP/Si interface (schematic of FIB cut shown on the left). In (a), a (220) bright field image, the GaP growth filled the V-groove and was stopped just prior to coalescence (WC195). In (b), a (220) dark field image, growth continued longer so that the GaP growing in neighboring grooves coalesced into a thin film. The images are to the same scale (WB989).

We have previously reported elevated TDD for coalesced samples without SiN_x caps,[41] along with pitting and associated planar defects above the (0 0 1) V-groove tops. In this work, we eliminated the pitting and associated planar defects by extending the length of the AsH_3 anneal prior to growth. This likely produces diatomic steps on the (0 0 1) tops,[50] eliminating possible APD formation; however, this improvement in surface morphology did not improve TDD. A possible explanation is that the caps prevent any (0 0 1) nucleation, thus preventing additional coalescence events between the GaP growing in and on top of the V-groove trenches as growth advances. Another potential explanation is the change in strain state at the top of the grooves—since the SiN_x caps are amorphous, there is no strained interface (no misfit dislocations, as can be visualized with virtual dislocations[43]) at the top of the V-grooves when there are caps. This may help avoid interacting dislocation strain fields leading to dislocation pinning and the inhibition of dislocation glide. Further study, perhaps on substrates with a smaller V-groove pitch and thus thinner GaP and more clearly visible misfit dislocations, is needed to understand this effect. Regardless of the mechanism, the caps are critical to maintaining a moderate TDD after coalescence, even when improvements to the surface pretreatment produce a suitable (0 0 1) Si growth surface from the perspective of APDs.

The lowest TDD we observed in coalesced GaP films on V-groove Si, 5×10^7 cm^{-2}, is still significantly above the level needed for optoelectronic devices. Recently, there have been a number of innovations in controlling TDD in III-V-on-Si heteroepitaxy,[2,4,5,7,10] and developing these techniques has largely relied on an understanding of the relaxation of the III-V layers as growth proceeds. In order to understand the strain relaxation process as growth proceeds, we used transmission electron microscopy (TEM) to image the GaP/Si interface to identify misfit dislocations.

Figure 5 shows cross-sectional TEM of focused ion beam (FIB) cuts made parallel to the V-grooves just before (a) and after (b) coalescence. In the case of Figure 5a, the lamella was taken from near the top of the groove, so the SiN_x cap is visible. The (1 1 1) GaP/Si interface passes through the (1 1 0) FIB cut at an angle, so misfit dislocations on the {1 1 1} sidewalls appear as diagonal lines in the cross-sectional TEM. Three misfit dislocation directions are possible on a given V-groove sidewall defined by the three 1 1 1 planes intersecting the fourth {1 1 1} plane of the V-groove sidewall. Two of these directions are at an angle to the grooves, and the third is parallel to the grooves. For the coalesced sample (Figure 5b), all three of these misfit dislocation orientations can be observed. However, before coalescence (Figure 5a), only one dislocation is observed, in approximately the same size of imaged area the GaP/Si interface. This, along with the misfits observed to continue across multiple grooves in the ECCI image in Figure 4, suggests that virtually all of the lattice relaxation in the GaP occurs after the film coalesces. Additional TEM images from FIB cuts taken perpendicular to the V-grooves can be found in the Supporting Information (S2).

The Matthews-Blakeslee critical thickness for dislocation glide for GaP grown on Si is around 40 nm, but experimentally, it is typically observed to not begin to relax until 45−95 nm of GaP has been grown.[51] In this work, the GaP growth completely filling the V-grooves is about 300 nm thick in the center of the groove, but at this stage of growth, it shows no misfit dislocations at the GaP/Si interface. This apparent increase in the GaP thickness that is needed to begin lattice relaxation through dislocation glide has a number of possible explanations. First, the V-groove structure has been computationally shown to increase critical thickness due to the different stress profile of growth in the trenches[44] and has been experimentally reported to affect strain relaxation.[52] Alternatively, the 3×1 surface reconstruction on the GaP could play a role: It creates a very smooth surface, which may create a higher barrier to dislocation half loop formation, inhibiting lattice relaxation by inhibiting dislocation nucleation. Regardless of the reason, this delay in relaxation is likely beneficial to the final material quality of the thin film. When relaxed islands of growth coalesce, grown-in sessile dislocations can form due to alignment errors between existing dislocations in neighboring islands;[43] however, here, the lack of relaxation in the V-grooves likely prevents such issues with grown-in dislocations,[21] so the population of dislocations present after the film relaxes will be largely glissile.

In conclusion, we have studied the morphology and dislocation dynamics of GaP as it coalesces into a thin film on V-groove Si. The width of the SiN_x caps was found to be the determining factor in the final morphology of the films, with narrow caps (100 nm wide) resulting in thin-film coalescence. This effect was traced to the influence of Si on the surface reconstruction of the epitaxial GaP, changing it from a standard 2×2/c4 $\times$ 2 reconstruction to a 3×1 reconstruction that is thought to stabilize the (0 0 1) facet. Narrow SiN_x caps likely allow the GaP to coalesce during a transient period where the V-groove Si sidewalls are covered, but the stabilizing influence of the Si remains on the (0 0 1) surface remains. Under conditions where coalescence occurs, AFM measurements showed a smooth surface with an R_q of 0.2 nm and visible atomic steps. ECCI showed that these films had

https://doi.org/10.1021/acsaelm.2c01688
ACS Appl. Electron. Mater. 2023, 5, 721−728

a TDD of 5 × 10^7 cm^{-2} shortly after coalescence, a moderate value that is still too high for most optoelectronic devices; the development of further dislocation reduction strategies is ongoing. TEM combined with the observation of misfit dislocations spanning many grooves further suggests that lattice relaxation occurs via dislocation glide after coalescence. The GaP exceeded the experimental critical thickness for GaP grown on planar Si by approximately a factor of 3, perhaps due to differing strain fields from the V-grooves or changes to the kinetics of dislocation half loop nucleation from the atypical 3 × 1 surface reconstruction. For these films to be useful as optoelectronic device templates, future work must focus on decreasing the TDD.

■ METHODS

V-groove Si substrates were prepared via nanoimprint lithography (NIL), as described in ref 38, with a pattern area of 1 × 1 cm^2. Such patterns can also be made over much larger areas using roll-to-plate NIL[53] or laser interference lithography.[54] To prevent growth on the (0 0 1)-oriented tops of the V-grooves, the SiN_x caps used for pattern definition were left on the top of the V-grooves.[41] To vary the geometry of the V-grooves (as in Figure 1), some samples were etched in HF prior to the removal of the microresist (mr-NIL210FC-500nm, NIL analogue to photoresist) mask to laterally etch the SiN_x caps, resulting in V-grooves with varying cap widths and thus varying distances needed for lateral overgrowth to result in coalescence.

Prior to growth, all samples were prepared with a wet chemical cleaning regimen of 30 s in 2% HF, 1 min in 4:1 H_2SO_4:H_2O_2 (piranha etch), and 15 s in 2% HF to produce a clean, hydrogen-terminated Si surface. All growths began with an As-based pretreatment anneal[50,55] as described in ref 38, but with an extended 20 min hold at 900 °C under AsH_3 to ensure complete cleaning of the surface. The GaP was nucleated and grown in a custom-built, vertical, atmospheric-pressure (620 torr) MOVPE reactor at optimized growth conditions of 800 °C and a V/III ratio of 5000 using AsH_3 and trimethylgallium (TMGa), as developed in prior work.[40,41]

SEM cross-sectional imaging was done with a Hitachi S-4800 SEM. ECCI[49,56] was performed on a Thermo Fisher Nova 630 SEM at 25 kV with a beam current of 3.2 nA using a vCD backscatter detector inserted under the pole piece to characterize misfit and threading dislocations in coalesced films. TEM cross-sectional images of select samples were taken with an FEI Tecnai ST30 TEM with an acceleration voltage of 300 kV.[57] The TEM cross sections were prepared using a FIB in an FEI Nova NanoLab 200 dual beam FIB workstation. AFM images of the coalesced material were taken with a Bruker D3100 AFM.

■ ASSOCIATED CONTENT

Supporting Information

The Supporting Information is available free of charge at https://pubs.acs.org/doi/10.1021/acsaelm.2c01688.

> **S1**: SEM of GaP on V-groove Si after 12 and 32 min of growth, as described in Figure 2. **S2**: Cross-sectional TEM of GaP on V-groove Si just before and after coalescence, as described in Figure 5 (PDF)

■ AUTHOR INFORMATION

Corresponding Author

Emily L. Warren − *National Renewable Energy Laboratory, Golden, Colorado 80401, United States;* orcid.org/0000-0001-8568-7881; Email: emily.warren@nrel.gov

Authors

Theresa E. Saenz − *National Renewable Energy Laboratory, Golden, Colorado 80401, United States; Department of Physics, Colorado School of Mines, Golden, Colorado 80401, United States;* orcid.org/0000-0002-7729-2051

John S. Mangum − *National Renewable Energy Laboratory, Golden, Colorado 80401, United States;* orcid.org/0000-0002-5926-7565

Olivia D. Schneble − *National Renewable Energy Laboratory, Golden, Colorado 80401, United States; Department of Physics, Colorado School of Mines, Golden, Colorado 80401, United States*

Anica N. Neumann − *National Renewable Energy Laboratory, Golden, Colorado 80401, United States; Department of Physics, Colorado School of Mines, Golden, Colorado 80401, United States*

Ryan M. France − *National Renewable Energy Laboratory, Golden, Colorado 80401, United States*

William E. McMahon − *National Renewable Energy Laboratory, Golden, Colorado 80401, United States;* orcid.org/0000-0001-5036-2032

Jeramy D. Zimmerman − *Department of Physics, Colorado School of Mines, Golden, Colorado 80401, United States;* orcid.org/0000-0001-8936-5345

Complete contact information is available at: https://pubs.acs.org/10.1021/acsaelm.2c01688

Notes

The authors declare the following competing financial interest(s): E.L.W., T.E.S., and J.D.Z. are inventors of patent 11120990, "Methods for depositing III-V compositions on silicon".

■ ACKNOWLEDGMENTS

The authors thank Jeff Carapella for III-V growth support, Patrick Walker for help with FIB TEM cross section preparation, Bobby To for AFM imaging, and Jacob Boyer for helpful discussions. This work was authored in part by the National Renewable Energy Laboratory, operated by Alliance for Sustainable Energy, LLC, for the U.S. Department of Energy (DOE) under Contract No. DE-AC36-08GO28308. Funding was provided by the U.S. Department of Energy Office of Energy Efficiency and Renewable Energy Solar Energy Technologies Office under award no. 34358 and 38261. The views expressed in the article do not necessarily represent the views of the DOE or the U.S. Government. The U.S. Government retains and the publisher, by accepting the article for publication, acknowledges that the U.S. Government retains a nonexclusive, paid-up, irrevocable, worldwide license to publish or reproduce the published form of this work, or allow others to do so, for U.S. Government purposes.

■ REFERENCES

(1) Supplie, O.; Romanyuk, O.; Koppka, C.; Steidl, M.; Nägelein, A.; Paszuk, A.; Winterfeld, L.; Dobrich, A.; Kleinschmidt, P.; Runge, E.; Hannappel, T. Metalorganic vapor phase epitaxy of III-V-on-silicon: Experiment and theory. *Prog. Cryst. Growth Charact.* **2018**, *64*, 103−132.

(2) Boyer, J. T.; Blumer, A. N.; Blumer, Z. H.; Lepkowski, D. L.; Grassman, T. J. Reduced Dislocation Introduction in III-V/Si Heterostructures with Glide-Enhancing Compressively Strained Superlattices. *Crys. Growth Des.* **2020**, *20*, 6939−6946.

(3) Boyer, J. T.; Blumer, A. N.; Blumer, Z. H.; Lepkowski, D. L.; Grassman, T. J. Correlation of early-stage growth process conditions with dislocation evolution in MOCVD-based GaP/Si heteroepitaxy. *J. Cryst. Growth* **2021**, *571*, 126251.

(4) Hool, R. D.; Chai, Y.; Sun, Y.; Eng, B. C.; Dhingra, P.; Fan, S.; Nay Yaung, K.; Lee, M. L. Challenges of relaxed n-type GaP on Si and strategies to enable low threading dislocation density. *Appl. Phys. Lett.* **2020**, *116*, 042102.

(5) Nandy, M.; Paszuk, A.; Feifel, M.; Koppka, C.; Kleinschmidt, P.; Dimroth, F.; Hannappel, T. A route to obtaining low-defect III-V epilayers on Si(100) utilizing MOCVD. *Crystal Growth & Design* **2021**, *21*, 5603−5613.

(6) Feifel, M.; Ohlmann, J.; France, R. M.; Lackner, D.; Dimroth, F. Electron channeling contrast imaging investigation of stacking fault pyramids in GaP on Si nucleation layers. *J. Cryst. Growth* **2020**, *532*, 125422.

(7) Shang, C.; Selvidge, J.; Hughes, E.; Norman, J. C.; Taylor, A. A.; Gossard, A. C.; Mukherjee, K.; Bowers, J. E. A Pathway to Thin GaAs Virtual Substrate on On-Axis Si (0 0 1) with Ultralow Threading Dislocation Density. physica status solidi (a). *physica status solidi (a)* **2021**, *218*, 2000402.

(8) Grassman, T. J.; Brenner, M. R.; Rajagopalan, S.; Unocic, R.; Dehoff, R.; Mills, M.; Fraser, H.; Ringel, S. A. Control and elimination of nucleation-related defects in GaP/Si(001) heteroepitaxy. *Appl. Phys. Lett.* **2009**, *94*, 232106.

(9) Volz, K.; Beyer, A.; Witte, W.; Ohlmann, J.; Nemeth, I.; Kunert, B.; Stolz, W. GaP-nucleation on exact Si (0 0 1) substrates for III/V device integration. *J. Cryst. Growth* **2011**, *315*, 37−47.

(10) Hool, R. D.; Sun, Y.; Li, B. D.; Dhingra, P.; Tham, R. W.; Fan, S.; Lee, M. L. Relaxed GaP on Si with low threading dislocation density. *J. Appl. Phys.* **2021**, *130*, 243104.

(11) Bioud, Y. A.; Boucherif, A.; Myronov, M.; Soltani, A.; Patriarche, G.; Braidy, N.; Jellite, M.; Drouin, D.; Ares, R. Uprooting defects to enable high-performance III-V optoelectronic devices on silicon. *Nature Comm.* **2019**, *10*, 4322.

(12) Feifel, M.; Lackner, D.; Schön, J.; Ohlmann, J.; Benick, J.; Siefer, G.; Predan, F.; Hermle, M.; Dimroth, F. Epitaxial GaInP/GaAs/Si Triple-Junction Solar Cell with 25.9% AM1.5g Efficiency Enabled by Transparent Metamorphic $Al_xGa_{1-x}As_yP_{1-y}$ Step-Graded Buffer Structures. *Sol. RRL* **2021**, *5*, 2000763.

(13) Fan, S.; Yu, Z. J.; Hool, R. D.; Dhingra, P.; Weigand, W.; Kim, M.; Ratta, E. D.; Li, B. D.; Sun, Y.; Holman, Z. C.; Lee, M. L. Current-Matched III-V/Si Epitaxial Tandem Solar Cells with 25.0% Efficiency. *Cell Rep. Phys. Sci.* **2020**, *1*, 100208.

(14) Lepkowski, D. L.; Grassman, T. J.; Boyer, J. T.; Chmielewski, D. J.; Yi, M. K.; Juhl, C.; Soeriyadi, A. H.; Western, N.; Mehrvarz, H.; Römer, U.; Ho-Baillie, A.; Kerestes, C.; Derkacs, D.; Whipple, S. G.; Stavrides, A. P.; Bremner, S. P.; Ringel, S. A. 23.4% monolithic epitaxial GaAsP/Si tandem solar cells and quantification of losses from threading dislocations. *Sol. Energy Mater. Sol. Cells* **2021**, *230*, 111299.

(15) Liang, D.; Bowers, J. E. Recent progress in lasers on silicon. *Nature Photonics* **2010**, *4*, 511−517.

(16) Chen, S.; Li, W.; Wu, J.; Jiang, Q.; Tang, M.; Shutts, S.; Elliott, S. N.; Sobiesierski, A.; Seeds, A. J.; Ross, I.; Smowton, P. M.; Liu, H. Electrically pumped continuous-wave III-V quantum dot lasers on silicon. *Nat. Photonics* **2016**, *10*, 307−311.

(17) Wan, Y.; Xiang, C.; Guo, J.; Koscica, R.; Kennedy, M.; Selvidge, J.; Zhang, Z.; Chang, L.; Xie, W.; Huang, D.; Gossard, A. C.; Bowers, J. E. High Speed Evanescent Quantum-Dot Lasers on Si. *Laser Photonics Rev.* **2021**, *15*, 2100057.

(18) Liao, M.; Chen, S.; Park, J.-S.; Seeds, A.; Liu, H. III-V quantum-dot lasers monolithically grown on silicon. *Semicond. Sci. Technol.* **2018**, *33*, 123002.

(19) Escobar Steinvall, S.; Stutz, E. Z.; Paul, R.; Zamani, M.; Dzade, N. Y.; Piazza, V.; Friedl, M.; de Mestral, V.; Leran, J.-B.; Zamani, R. R.; Fontcuberta i Morral, A. Towards defect-free thin films of the earth-abundant absorber zinc phosphide by nanopatterning. *Nanoscale Advances* **2021**, *3*, 326−332.

(20) Yuan, X.; Pan, D.; Zhou, Y.; Zhang, X.; Peng, K.; Zhao, B.; Deng, M.; He, J.; Tan, H. H.; Jagadish, C. Selective area epitaxy of III-V nanostructure arrays and networks: Growth, applications, and future directions. *Applied Physics Reviews* **2021**, *8*, 021302.

(21) Mangum, J. S.; Theingi, S.; Steiner, M. A.; McMahon, W. E.; Warren, E. L. Development of High-Efficiency GaAs Solar Cells Grown on Nanopatterned GaAs Substrates. *Cryst. Growth Des.* **2021**, *21*, 5955−5960.

(22) Oshima, T.; Oshima, Y. Selective area growth of -Ga $_2$O $_3$ by HCl-based halide vapor phase epitaxy. *Applied Physics Express* **2022**, *15*, 075503.

(23) Oh, J.; Ryu, J.; Yang, D.; Lee, S.; Kim, J.; Hwang, K.; Hwang, J.; Kim, D.; Park, Y.; Yoon, E.; Jang, H. W. Selective Area Growth of GaN Using Polycrystalline γ-Alumina as a Mask for Discrete Micro-GaN Array. *Crystal Growth & Design* **2022**, *22*, 1770−1777.

(24) Schneble, O. D.; Neumann, A. N.; Mangum, J. S.; Norman, A. G.; Warren, E. L.; Zimmerman, J. D. Application of templated vapor-liquid-solid growth to heteroepitaxy of InP on Si. *J. Vac. Sci. Technol. A* **2021**, *39*, 013404.

(25) Li, Q.; Lau, K. M. Epitaxial growth of highly mismatched III-V materials on (0 0 1) silicon for electronics and optoelectronics. *Prog. Cryst. Growth Char. Mater.* **2017**, *63*, 105−120.

(26) Kunert, B.; Mols, Y.; Baryshniskova, M.; Waldron, N.; Schulze, A.; Langer, R. How to control defect formation in monolithic III/V hetero-epitaxy on (100) Si? A critical review on current approaches. *Semicond. Sci. Technol.* **2018**, *33*, 093002.

(27) Li, Q.; Ng, K. R.; Lau, K. M. Growing antiphase-domain-free GaAs thin films out of highly ordered planar nanowire arrays on exact (001) silicon. *Appl. Phys. Lett.* **2015**, *106*, 072105.

(28) Vaisman, M.; Jain, N.; Li, Q.; Lau, K. M.; Makoutz, E.; Saenz, T.; McMahon, W. E.; Tamboli, A. C.; Warren, E. L. GaAs Solar Cells on Nanopatterned Si Substrates. *IEEE J. Photovolt.* **2018**, *8*, 1635−1640.

(29) Shi, B.; Wang, L.; Taylor, A. A.; Suran Brunelli, S.; Zhao, H.; Song, B.; Klamkin, J. MOCVD grown low dislocation density GaAs-on-V-groove patterned (001) Si for 1.3 μm quantum dot laser applications. *Appl. Phys. Lett.* **2019**, *114*, 172102.

(30) Norman, J.; Kennedy, M. J.; Selvidge, J.; Li, Q.; Wan, Y.; Liu, A. Y.; Callahan, P. G.; Echlin, M. P.; Pollock, T. M.; Lau, K. M.; Gossard, A. C.; Bowers, J. E. Electrically pumped continuous wave quantum dot lasers epitaxially grown on patterned, on-axis (0 0 1) Si. *Optics Express* **2017**, *25*, 3927.

(31) Ismail, K.; Legoues, F.; Karam, N. H.; Carter, J.; Smith, H. I. High-quality GaAs on sawtooth-patterned Si substrates. *Appl. Phys. Lett.* **1991**, *59*, 2418.

(32) Kim, Y.; Yudistira, D.; Kunert, B.; Baryshnikova, M.; Alcotte, R.; Ozdemir, C. I.; Kim, S.; Lardenois, S.; Verheyen, P.; Van Campenhout, J.; Pantouvaki, M. Monolithic GaAs/Si V-groove depletion-type optical phase shifters integrated in a 300 mm Si photonics platform. *Photonics Research* **2022**, *10*, 1509.

(33) Han, Y.; Xue, Y.; Lau, K. M. Selective lateral epitaxy of dislocation-free InP on silicon-on-insulator. *Appl. Phys. Lett.* **2019**, *114*, 192105.

(34) Han, Y.; Li, Q.; Ng, K. W.; Zhu, S.; Lau, K. M. InGaAs/InP quantum wires grown on silicon with adjustable emission wavelength at telecom bands. *Nanotechnology* **2018**, *29*, 225601.

(35) Wang, Z.; Tian, B.; Pantouvaki, M.; Guo, W.; Absil, P.; Van Campenhout, J.; Merckling, C.; Van Thourhout, D. Room-temperature InP distributed feedback laser array directly grown on silicon. *Nat. Photonics* **2015**, *9*, 837−842.

(36) Paladugu, M.; Merckling, C.; Loo, R.; Richard, O.; Bender, H.; Dekoster, J.; Vandervorst, W.; Caymax, M.; Heyns, M. Site Selective Integration of III-V Materials on Si for Nanoscale Logic and Photonic Devices. *Cryst. Growth Des.* **2012**, *12*, 4696−4702.

(37) Li, Q.; Lai, B.; Lau, K. M. Epitaxial growth of GaSb on V-grooved Si (001) substrates with an ultrathin GaAs stress relaxing layer. *Appl. Phys. Lett.* **2017**, *111*, 172103.

(38) Saenz, T. E.; McMahon, W. E.; Norman, A. G.; Perkins, C. L.; Zimmerman, J. D.; Warren, E. L. High-Temperature Nucleation of GaP on V-Grooved Si. *Crys. Growth Des.* **2020**, *20*, 6745−6751.

(39) Warren, E. L.; Makoutz, E.; Saenz, T.; Martirossyan, M.; Neumann, A.; Horowitz, K.; Matheson, A.; Norman, A.; Tamboli, A. C.; Zimmerman, J. D.; McMahon, W. E. Enabling low-cost III-V/Si

https://doi.org/10.1021/acsaelm.2c01688
ACS Appl. Electron. Mater. 2023, 5, 721−728

integration through nucleation of GaP on v-grooved Si substrates. *2018 IEEE 7th World Conference on Photovoltaic Energy Conversion (WCPEC)*, Waikoloa, Hawaii, United States, 2018; pp 268−270. .

(40) Saenz, T. E.; McMahon, W. E.; Norman, A. G.; Perkins, C. L.; Zimmerman, J. D.; Warren, E. L. Nucleation of high-quality GaP on Si through v-groove Si substrates. *2020 47th IEEE Photovoltaic Specialists Conference (PVSC)*, Calgary, AB, Canada, 2020; pp 0352−0353. .

(41) Saenz, T. E.; Mangum, J. S.; Schneble, O. D.; Garcia, I.; France, R. M.; McMahon, W. E.; Zimmerman, J. D.; Warren, E. L. Towards a III-V solar cell with a metamorphic graded buffer directly grown on v-groove Si substrates. *2021 IEEE 48th Photovoltaic Specialists Conference (PVSC)*, Fort Lauderdale, Florida, United States, 2021; pp 1921−1924. .

(42) Lee, S. C.; Huffaker, D. L.; Brueck, S. R. J. Faceting of a quasi-two-dimensional GaAs crystal in nanoscale patterned growth. *Appl. Phys. Lett.* **2008**, *92*, 023103.

(43) McMahon, W. E.; Vaisman, M.; Zimmerman, J. D.; Tamboli, A. C.; Warren, E. L. Perspective: Fundamentals of coalescence-related dislocations, applied to selective-area growth and other epitaxial films. *APL Mater.* **2018**, *6*, 120903.

(44) Freund, L. B.; Gosling, T. J. Critical thickness condition for growth of strained quantum wires in substrate V-grooves. *Appl. Phys. Lett.* **1995**, *66*, 2822−2824.

(45) Dede, D.; Glas, F.; Piazza, V.; Morgan, N.; Friedl, M.; Guniat, L.; Nur Dayi, E.; Balgarkashi, A.; Dubrovskii, V. G; Fontcuberta i Morral, A. Selective area epitaxy of GaAs: the unintuitive role of feature size and pitch. *Nanotechnology* **2022**, *33*, 485604.

(46) McMahon, W. E.; Warren, E. L.; Kibbler, A. E.; France, R. M.; Norman, A. G.; Reedy, R. C.; Olson, J. M.; Tamboli, A. C.; Stradins, P. Surfaces and interfaces governing the OMVPE growth of APD-free GaP on AsH3-cleaned vicinal Si(100). *J. Cryst. Growth* **2016**, *452*, 235−239.

(47) Ruhstorfer, D.; Döblinger, M.; Riedl, H.; Finley, J. J.; Koblmüller, G. Role of twin defects on growth dynamics and size distribution of undoped and Si-doped GaAs nanowires by selective area epitaxy. *J. Appl. Phys.* **2022**, *132*, 204302.

(48) Yamaguchi, M.; Amano, C. Efficiency calculations of thin-film GaAs solar cells on Si substrates. *J. Appl. Phys.* **1985**, *58*, 3601.

(49) Carnevale, S. D.; Deitz, J. I.; Carlin, J. A.; Picard, Y. N.; De Graef, M.; Ringel, S. A.; Grassman, T. J. Rapid misfit dislocation characterization in heteroepitaxial III-V/Si thin films by electron channeling contrast imaging. *Appl. Phys. Lett.* **2014**, *104*, 232111.

(50) Warren, E. L.; Kibbler, A. E.; France, R. M.; Norman, A. G.; Stradins, P.; McMahon, W. E. Growth of antiphase-domain-free GaP on Si substrates by metalorganic chemical vapor deposition using an in situ AsH_3 surface preparation. *Appl. Phys. Lett.* **2015**, *107*, 082109.

(51) Takagi, Y.; Furukawa, Y.; Wakahara, A.; Kan, H. Lattice relaxation process and crystallographic tilt in GaP layers grown on misoriented Si(001) substrates by metalorganic vapor phase epitaxy. *J. Appl. Phys.* **2010**, *107*, 063506.

(52) Guo, W.; Mols, Y.; Belz, J.; Beyer, A.; Volz, K.; Schulze, A.; Langer, R.; Kunert, B. Anisotropic relaxation behavior of InGaAs/GaAs selectively grown in narrow trenches on (001) Si substrates. *J. Appl. Phys.* **2017**, *122*, 025303.

(53) Ahn, S. H.; Guo, L. J. Large-Area Roll-to-Roll and Roll-to-Plate Nanoimprint Lithography: A Step toward High-Throughput Application of Continuous Nanoimprinting. *ACS Nano* **2009**, *3*, 2304−2310.

(54) Bläsi, B.; Müller, M.; Rossmeier, H. Resource-efficient generation of large-area micro and nanostructures: High-quality, large area diffraction gratings originated by diode laser-driven interference lithography. *PhotonicsViews* **2023**, *20*, 64−67.

(55) Saenz, T. E.; Nandy, M.; Paszuk, A.; Ostheimer, D.; Koch, J.; McMahon, W. E.; Zimmerman, J. D.; Hannappel, T.; Warren, E. L. MOCVD surface preparation of V-groove Si for III-V growth. *J. Cryst. Growth* **2022**, *597*, 126843.

(56) Mangum, J. S.; Theingi, S.; Neumann, A. N.; McMahon, W. E.; Warren, E. L. Using electron channeling contrast imaging to inform and improve the growth of high-efficiency GaAs solar cells on nanopatterned GaAs substrates. *J. Cryst. Growth* **2022**, *581*, 126490.

(57) Preibisch, S.; Saalfeld, S.; Tomancak, P. Globally optimal stitching of tiled 3D microscopic image acquisitions. *Bioinform.* **2009**, *25*, 1463−1465.